ELSEVIER

Effect of an electromagnetic field on natural convection in an inclined porous layer

W. Bian, P. Vasseur, E. Bilgen, and F. Meng
Mechanical Engineering Department, Ecole Polytechnique, University of Montreal, Montreal, PQ, Canada

An investigation is conducted to study the effect of an electromagnetic field on free convection of in inclined rectangular porous cavity saturated with an electrically conducting fluid. The enclosure has the long side walls heated isothermally, while the short ends are thermally insulated. A uniform magnetic field is applied normal to the heated walls. The porous medium, modeled according to Darcy's law, is assumed to be isotropic. The dimensionless governing equations are derived in terms of the characteristic dimensionless parameters; namely, the Rayleigh number R, the magnetic Hartmann number Ha, the cavity aspect ratio A, and the inclination angle θ. An approximate analytical solution is presented for the boundary-layer flow regime within a vertical cavity. A linear stability analysis is made to determine the effect of the magnetic field on the onset of convection in a horizontal layer heated from below. A numerical study is performed to assess and extend the results of the analytical solutions. It is found that with application of an external magnetic field, the temperature and velocity fields are significantly modified.

Introduction

Natural convection in a rectangular porous cavity heated from the side has received considerable attention in recent years because of its applications in many engineering areas. A number of studies analyzing this problem model the system as a two-dimensional (2-D) layer framed by two horizontal adiabatic walls and two vertical isothermal walls. These studies have reported extensive theoretical (Walker and Homsy 1978; Simpkins and Blythe 1980), numerical (Shiralkar et al. 1983; Prasad and Kulacki 1984) and experimental (Klarsfeld 1970; Seki et al. 1978) results with regard to the flow and heat transfer characteristics of the porous layer. The state of the art has been summarized in a recent book by Nield and Bejan (1992).

Most existing studies are concerned with the natural convection heat transfer through a porous medium saturated by an electrically nonconducting fluid, which is the case in most practical situations. Recently, the equally important problem of hydromagnetic convective flow of a conducting fluid through a porous medium has been investigated. When an electrically conducting fluid is subjected to a magnetic field, the fluid motion induces an electric current and, in general, the fluid velocity is reduced due to interaction between the electric current and the motion. Very little has been done on the natural convection of electrically conducting fluids in porous media in the presence of a magnetic field, despite its potential applications. For instance, the study of the interaction of the geomagnetic field with the fluid in the geothermal region, where the Earth's crust serves as a porous medium, is of great importance to geophysicists. Also, in metallurgical applications involving continuous casting, the solidification structure can be improved by electromagnetic stirring to obtain a fine-grained structure to get better final mechanical properties. For dendritic solidification of alloys, dendrites in the mushy zone can be viewed as a porous medium.

The interaction of an external magnetic field with convection currents in a porous medium was apparently first considered by Raptis et al. (1982a, 1982b). They studied (Raptis et al. 1982a) the influence of a horizontal constant magnetic field upon the free convective flow through a porous medium occupying a semi-infinite region of the space bounded by two vertical infinite surfaces. Raptis et al. (1982b) further extended their investigation to study the free convection flow of a conducting fluid through a porous medium bounded by two horizontal plates. Singh and Dikshit (1987) studied the free convection of the Couette motion of an electrically conducting fluid through a porous medium. Exact solutions for the velocity field, skin-friction, and the volume flux of the fluid were obtained in terms of the governing parameters of the problem. Kumar Jha and Prasad (1991) studied the heat source characteristics on the free-convection and mass transfer flow past an impulsively started infinite vertical plate bounding a saturated porous medium under the action of a magnetic field. Effects of various parameters on the velocity field were extensively discussed. An analysis of the effects of Hall current on hydromagnetic free-convective flow through a porous medium bounded by a vertical plate has been theoretically investigated by Takhar and Ram (1992). A strong magnetic field was imposed in a direction perpendicular to the free stream and inclined with an angle α to the vertical direction. The influence of Hall currents on the flow was studied for various values of α. Recently, Ni et al. (1993) investigated the effect of an electromagnetic field on steady natural convection in a vertical enclosure filled with a porous medium.

In the present study, an investigation is conducted to examine the effect of an electromagnetic field on two-dimensional 2-D

Address reprint requests to Mr. W. Bian, Department of Mechanical Engineering, Ecole Polytechnique, C.P. 6079, Succ. Centre-Ville, Montreal, P.Q. GOA 1AO, Canada.

Received 18 February 1995; accepted 24 July 1995

Int. J. Heat and Fluid Flow 17: 36–44, 1996

655 Avenue of the Americas, New York, NY 10010

0142-727X/96/$15.00
SSDI 0142-727X(95)00070-7

natural convection in an inclined slot filled with an isotropic porous medium saturated by an electrically conducting fluid. The magnetic field is applied perpendicularly to the long side walls of the cavity, which are differentially heated. In the special case of a vertical enclosure, an analytical Oseen-linearized solution for the boundary-layer regime is presented. When the cavity is inclined, the problem becomes more complicated and is studied through numerical simulations. The influences of the governing parameters on the fluid flow and heat transfer characteristics are well established.

Mathematical formulation

The physical model considered in this paper is shown in Figure 1. A two-dimensional (2-D) inclined rectangular enclosure of height H and width L is filled with a porous medium saturated by an electrically conducting fluid. The two long side walls are maintained at temperatures T'_H and T'_C, respectively, while the short end walls are thermally insulated. A uniform and constant magnetic field $\mathbf{B}'$ is applied normal to the heated sides of the cavity. The fluid in this enclosure experiences the mechanism of buoyancy, due to fluid density changes caused by temperature variations resulting from heat transfer and the interaction of the magnetic field with the convective motion. The magnetic Reynolds number is assumed to be small so that the induced magnetic field can be neglected compared to the applied magnetic field (Garandet et al. 1992).

The equations governing the conservation of mass, momentum, energy, and electric charge transfer for laminar flow are written as follows:

$$\nabla \cdot \mathbf{V}' = 0 \tag{1}$$

$$\frac{\mu}{K}\mathbf{V}' = -\nabla p' + \rho \mathbf{g} + \mathbf{J}' \times \mathbf{B}' \tag{2}$$

$$\mathbf{V}' \cdot \nabla T' = \alpha_f \nabla^2 T' \tag{3}$$

$$\nabla \cdot \mathbf{J} = 0 \; ; \; \mathbf{J}' = \sigma(-\nabla\phi + \mathbf{V}' \times \mathbf{B}') \tag{4}$$

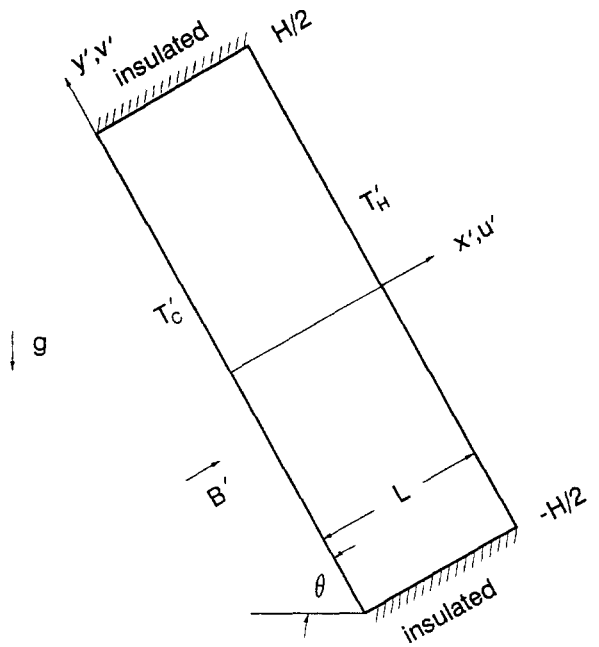

Figure 1 Schematic of the problem

These equations correspond to having the porous medium modeled according to Darcy's law. The porous medium is assumed to be hydrodynamically, thermally, and electrically isotropic and saturated with a fluid that is in local thermodynamic equilibrium with the solid matrix. Both viscous dissipation and Joulean energy dissipation are neglected.

As discussed by Garandet et al. (1992), for a 2-D, steady-state situation, Equation 4 for the electric potential reduces to $\nabla^2\phi = 0$. The unique solution is $\nabla\phi = 0$, because there is always somewhere around the enclosure an electrically insulating boundary on which $\partial\phi/\partial n = 0$, which means that the electric field vanishes

Notation

A	aspect ratio, H/L
$\mathbf{B}'$	applied magnetic field
g	acceleration due to gravity
H	height of the cavity
Ha	Hartmann number, $B'(K\sigma/\mu)^{1/2}$
$\mathbf{J}'$	electric current density
k	effective thermal conductivity of saturated liquid and porous medium
K	permeability of fluid-saturated porous medium
l	characteristic length, Equation 19
L	thickness of the cavity
Nu	Nusselt number, Equation 9
p'	pressure
R	Darcy-Rayleigh number, $Kg\beta L\Delta T'/\alpha_f \nu$
T	dimensionless temperature, $(T' - T'_C)/\Delta T'$
$\Delta T'$	characteristic temperature, $(T'_H - T'_C)$
V'	velocity field
u, v	dimensionless velocities in x and y directions, $(u', v')L/\alpha_f$
x, y	dimensionless cartesian coordinates, $(x', y')/L$

Greek

α	wavelength
α_f	effective thermal diffusivity
β	coefficient of thermal expansion of the fluid
θ	inclination angle
μ	dynamic viscosity of the fluid
ν	kinematic viscosity of the fluid
ρ	fluid density
σ	electrical conductivity
ϕ	electric potential
ψ	dimensionless stream function, ψ'/α_f
Φ	dimensionless temperature, Equation 22
Ψ	dimensionless stream function, Equation 22

Superscripts

$'$	dimensional quantities
$*$	dimensionless variables, Equation 19
$\hat{}$	perturbations from the rest state

Subscripts

c	cold isothermal boundary
cr	critical value for the onset of convection
H	hot isothermal boundary
max	maximum value

everywhere. The Lorentz force then reduces to a systematically damping factor.

Scaling length, velocity, and temperature with L, α_f/L and $\Delta T' = T'_H - T'_C$, and elimination the pressure term in Equation 2 in the usual way, it is readily shown that the dimensionless governing equations can be expressed as follows:

$$(1 + \mathrm{Ha}^2)\frac{\partial^2\psi}{\partial x^2} + \frac{\partial^2\psi}{\partial y^2} = -\mathrm{R}\left(\frac{\partial T}{\partial x}\sin\theta - \frac{\partial T}{\partial y}\cos\theta\right) \tag{5}$$

$$\nabla^2 T = \frac{\partial\psi}{\partial y}\frac{\partial T}{\partial x} - \frac{\partial\psi}{\partial x}\frac{\partial T}{\partial y} \tag{6}$$

where ψ is a dimensionless stream function defined as follows:

$$u = \frac{\partial\psi}{\partial y}\ ;\ v = -\frac{\partial\psi}{\partial x} \tag{7}$$

so that Equation 1 is identically satisfied.

The nondimensional boundary conditions over the walls of the enclosure are as follows:

$$\begin{cases} \psi = 0 & T = 0 \quad \text{on} \quad x = 0 \\ \psi = 0 & T = 1 \quad \text{on} \quad x = 1 \\ \psi = 0 & \dfrac{\partial T}{\partial y} = 0 \quad \text{on} \quad y = \pm A/2 \end{cases} \tag{8}$$

where $A = H/L$ is the cavity aspect ratio.

The overall heat transfer rate across the enclosure is expressed by the average Nusselt number defined as follows:

$$\mathrm{Nu} = \frac{1}{A}\int_{-A/2}^{A/2}\left.\frac{\partial T}{\partial x}\right|_{x=0} \mathrm{d}y \tag{9}$$

The present problem is dependent on the parameters R, Ha, A, and θ. Ranges of these physical parameters are selected to explore the effects of the magnetic field on natural convection in porous media.

Numerical method

Numerical solutions of the full conservation equations are obtained using the control-volume finite difference method described by Patankar (1980). A power-law scheme is adopted for the convection–diffusion formulation. The discretized equations obtained are solved iteratively, using a line-by-line application of the Thomas algorithm. The numerical procedure starts with determining the temperature field T by solving the energy Equation 6. Next, the momentum Equation 5 is solved for ψ using a known temperature distribution. Finally, the velocity components are evaluated, for points that lie on the faces of each elementary control volume, using Equation 7.

Nonuniform grid spacing is used in the x-direction. Grid spacing is minimum near a heated wall and is increased away from the wall up to the center of the cavity. Uniform mesh spacing is used in the y-direction. Trial calculations were necessary in order to optimize computation time and accuracy. Convergence was verified by employing coarser and finer grids on selected test problems. During the program tests, 61×41, 61×61, and 81×81 grids were used. Because of minor differences (less than 1%) and to save on computation cost, the results presented here are obtained with 61×41 for a cavity with an aspect ratio $A = 4$ and 61×61 with $A = 8$. The criterion used for the iterative convergence is as follows:

$$\max\frac{|f_{i,j\,\mathrm{new}} - f_{i,j\,\mathrm{old}}|}{|f_{i,j\,\mathrm{old}}|} < r_f \tag{10}$$

were $f_{i,j}$ stands for temperature and stream function, and r_f has been taken as 10^{-6} for both ψ and T.

Prior to calculations, checks were conducted to validate the calculation procedure by reference to the flow of a vertical porous enclosure. In the limiting case of no magnetic field (Ha = 0), some of the cases considered by Shiralkar et al. (1983) were reproduced. In general, it was found that essentially identical flow and temperature patterns as well as Nusselt number were obtained. For instance when R = 500 and $A = 5.0$, an overall Nusselt number of 5.02 was obtained in the present study, while that reported by Lauriat and Prasad (1987) was 4.92. As an additional check on the accuracy of the results, the convergence of the numerical solutions was checked by performing overall energy conservations.

Results and discussion

In this section the results of the numerical study are discussed in order to understand the natural convection of an electrically conducting fluid in an inclined porous enclosure in the presence of a magnetic field. The non-dimensional parameters are the Rayleigh number R, the Hartmann number Ha, the aspect ratio A, and the inclination angle θ. In the present study $A = 4$ and 8. Computations are carried out for R ranging from 2×10^2 to 5×10^3, Ha ranging from 0 to 10 and $0° \le \theta \le 180°$. Changes in field characteristics due to combined effect of buoyancy and applied magnetic field are discussed in detail. Effects of the magnetic field on the average Nusselt number are also discussed. First, the case of a vertical cavity is considered. Then, the case of a horizontal layer heated from below is studied. Finally, we investigate the influence of the inclination of the layer on the present problem.

The vertical layer heated from the sides

In this section, we consider the influence of a magnetic field on temperature and flow distributions within a vertical enclosure ($\theta = 90°$). Figures 2a–d show typical contour maps of temperature and stream function obtained numerically for R = 500, $A = 4$, and various values of Ha. In all these graphs, the increments between adjacent streamlines and isotherms are $\delta\psi = \psi_{\max}/10$ and $\delta T = 0.1$ where $\psi_{\max}$ is the maximum value of the stream function. The influence of a magnetic field on flow and temperature distributions is apparent from these figures. In the absence of a magnetic field, the flow and temperature fields of Figure 2a are similar to the results obtained in the past by many investigators (see for instance Nield and Bejan 1992). Thus, the flow field comprises a unicellular flow of relatively high velocity, circulating around the entire cavity. Because of boundary-layer effects, the temperature field is characterized by sharp drops in temperature near the vertical walls. It is interesting to note that, if the magnetic field is relatively strengthened, the flow circulation is progressively inhibited by the retarding effect of the electromagnetic body force. Thus, the maximum intensity of circulation is $\psi_{\max} = 31.069$ for Ha = 0 but is only $\psi_{\max} = 0.619$ for Ha = 10. For large Ha, Figure 2d indicates that the convection is almost suppressed, and the isotherms are nearly parallel to the vertical wall, indicating that a quasiconduction regime is reached. Finally, it is observed from Figure 2 that, although the thicknesses of the vertical boundary layers increase with Ha, the opposite effect is observed for the flow upon the horizontal walls. Thus, the flow pattern in Figure 2d is characterized by a weak vertical flow but a very strong horizontal flow through very thin hydrodynamic boundary layers near the horizontal walls.

In general, the quantities of interest involved in the present problem are related in a way so complicated that estimations of their orders of magnitudes by scale analysis are almost impossi-

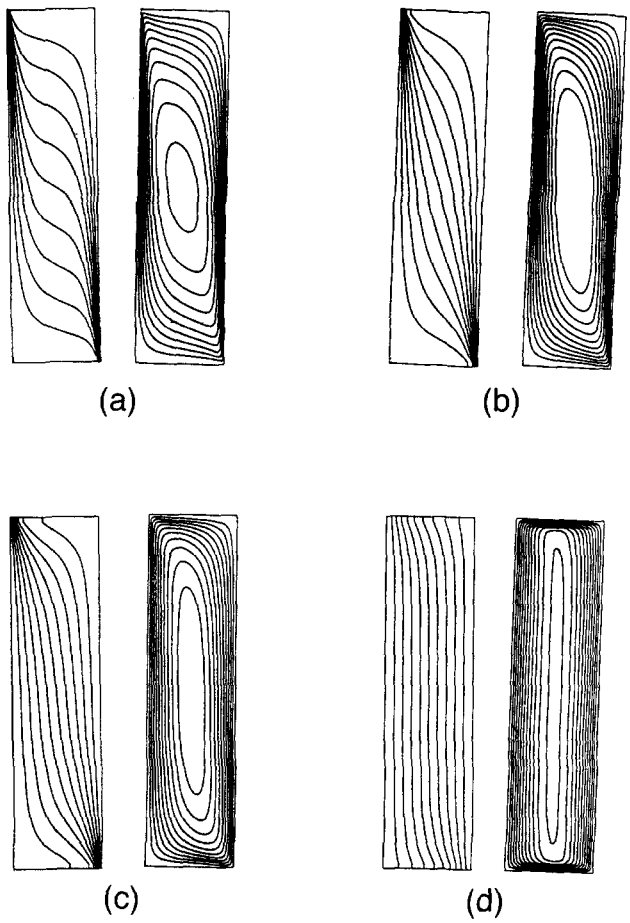

Figure 2 Computed contour maps of the isothermal lines and streamfunction for $A = 4$, $\theta = 90°$, $R = 500$, and a) $Ha = 0$, $\psi_{max} = 31.069$; b) $Ha = 1.7$, $\psi_{max} = 12.948$; c) $Ha = 3$, $\psi_{max} = 6.033$; d) $Ha = 10$, $\psi_{max} = 0.619$

ble. However, for a vertical cavity with the limiting case of boundary-layer flow regime, order of magnitude estimates can be derived on scaling grounds.

In the boundary-layer regime; i.e., when $R \gg 1$, most of the fluid motion is restricted to a thin layer δ' along each vertical wall. Recognizing δ' and H as the x' and y' scales in the boundary-layer region of interest ($\delta' \ll H$) the conservation Equations 5 and 6 require the following balances:

$$(1 + Ha^2)\frac{v}{\delta} \sim R\frac{\Delta T}{\delta} \tag{11}$$

$$v\frac{\Delta T}{A} \sim \frac{\Delta T}{\delta^2} \tag{12}$$

where $\delta = (\delta'/H)$ is the dimensionless thickness of the horizontal boundary layer, and ΔT is the dimensionless temperature difference across the boundary layer. Obviously, from the thermal boundary conditions, Equation 8, $\Delta T \sim 1$.

Solving the balance equations for v and δ we obtain the following:

$$\delta \sim \left[A(1 + Ha^2)/R\right]^{1/2} \tag{13}$$

$$v \sim R/(1 + Ha^2) \tag{14}$$

The order of magnitude of the velocity component u is obtained from the continuity Equation 1 as follows:

$$u \sim \frac{v\delta}{A} \sim \left[R/\left(A(1 + Ha^2)\right)\right]^{1/2} \tag{15}$$

The scale for the stream function can be obtained from Equation 7 as follows:

$$\psi \sim \left[R\,A/(1 + Ha^2)\right]^{1/2} \tag{16}$$

The total heat transfer rate from one side wall to the other is given by the following:

$$q' \sim kH\frac{\Delta T'}{\delta'} \tag{17}$$

The average Nusselt number, defined as the total heat transfer over the pure heat conduction through the cavity, has the following scale:

$$Nu = \frac{q'}{q'_c} = \frac{kH\Delta T'/\delta'}{kH\Delta T'/L} \sim \frac{1}{A^{1/2}}\frac{R^{1/2}}{(1 + Ha^2)^{1/2}} \tag{18}$$

in which $q'_c = kH\Delta T'/L$ is the heat transfer in the pure-conduction limit.

In the absence of a magnetic field ($Ha = 0$), the scales above reduce to those predicted Bejan (1985) while studying the boundary-layer regime within a porous cavity heated isothermally from the sides. The results above are expected to be valid only when the vertical boundary layers are slender ($\delta' \ll H$); i.e., for $R/(1 + Ha^2) \gg 1$. Also, the vertical boundary layers must be distinct ($\delta' \ll L$), which requires that $[R/(1 + Ha^2)]^{1/2} \gg A^{1/2}$.

The boundary-layer approximations to the governing equations can now be obtained from the results of the above order-of-magnitude analysis. When the following dimensionless variables are used:

$$\begin{cases} x^* = \dfrac{x'}{l} & y^* = \dfrac{y'}{H} & \psi^* = \dfrac{\psi'}{\alpha_f}\dfrac{l}{H} \\ u^* = \dfrac{u'l}{\alpha_f} & v^* = \dfrac{v'l^2}{\alpha_f H} & T^* = \dfrac{T' - T_c}{\Delta T'} \\ l^2 = \dfrac{LH}{R/(1 + Ha^2)} \end{cases} \tag{19}$$

the approximate forms of Equations 5 and 6 can be obtained as follows:

$$\frac{\partial v^*}{\partial x^*} = \frac{\partial T^*}{\partial x^*} \tag{20}$$

$$u^*\frac{\partial T^*}{\partial x^*} + v^*\frac{\partial T^*}{\partial y^*} = \frac{\partial^2 T^*}{\partial x^{*2}} \tag{21}$$

Defining the boundary-layer variables as (Gill 1966)

$$\begin{cases} T^* = T_0(y^*) + \Phi(x^*, y^*) \\ \psi^* = \psi_0(y^*) + \Psi(x^*, y^*) \end{cases} \tag{22}$$

where Φ and $\Psi \to 0$ as $x^* \to \infty$, we can establish the necessary boundary conditions

$$\begin{cases} \text{at} \quad x^* = 0, \quad \psi^* = 0 \quad T^* = 0 \\ \text{at} \quad x^* \to \infty, \quad \psi^* = \psi_0(y^*) \quad T^* = T_0(y^*) \end{cases} \tag{23}$$

In the above equations $\psi_0(y^*)$ and $T_0(y^*)$ are the dimensionless stream function and temperature distribution within the core of the cavity.

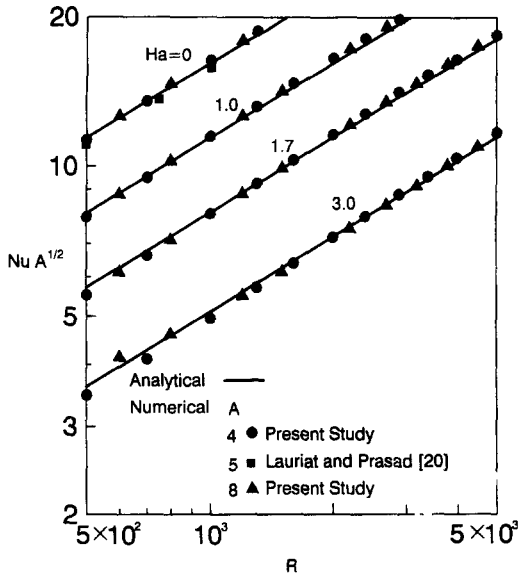

Figure 3 Effect of the Rayleigh number on the Nusselt number for $\theta = 90°$ and various values of the Hartmann number

The dimensionless nonlinear governing Equations 20–21 and the boundary conditions 23 are exactly the same as those derived by Weber (1975) and Simpkins and Blythe (1980) while studying boundary-layer flows within a porous layer in the absence of a magnetic field (Ha = 0). The analytical results obtained by Simpkins and Blythe, on the basis of an integral relation approach, are used here, because they proved to be in excellent agreement with numerical solutions of the boundary-layer equations. Translating their results in our notation, it is readily found that, for the present problem, the average Nusselt number is given by the following:

$$\mathrm{Nu} = 0.51\left[\frac{\mathrm{R}}{A(1+\mathrm{Ha}^2)}\right]^{1/2} \tag{24}$$

Figure 3 shows the dependence of the Nusselt number Nu on the Rayleigh and Hartmann numbers. Results are presented for $5 \times 10^2 \leq \mathrm{R} \leq 5 \times 10^3$ for which a boundary-layer flow regime prevails. The analytical results, Equation 24, are continuous lines; numerical results obtained for $A = 4$ and 8, shown as solid symbols, are seen to agree well. In the absence of a magnetic field, Equation 24 reduces to $\mathrm{Nu} = 0.51(\mathrm{R}/A)^{1/2}$ as predicted by Simpkins and Blythe (1980). For this situation, the numerical results obtained in the past by Lauriat and Prasad (1987) for $A = 5$ are also indicated in the graph for comparison.

Another view of the effect of Ha on the heat transfer is found in Figure 4 where Nu is plotted as a function of Ha for R = 200, 500, and 1500. The numerical results, obtained for $A = 4$, are depicted by the solid lines, and the dashed lines represent the boundary-layer regime, Equation 24. For a given Rayleigh number, when Ha is relatively small, the flow is in the boundary-layer regime, and the numerically predicted Nusselt number is in good agreement with the analytical solution. The boundary layer regime prevails up to a given value of Ha, above which this regime ends because of the progressively retarding effect of the electromagnetic body force. As the value of Ha is made larger, the strength of the convective motion is progressively suppressed, and the boundary-layer regime is followed by the asymptotic and conduction regime for which $\mathrm{Nu} \to 1$. Naturally, the Hartmann number ranges for asymptotic and conduction regimes are also extended as R is made larger.

The horizontal layer heated from below

The effect of a magnetic field on the Benard convection in a horizontal layer heated from below ($\theta = 180°$) is now considered. For this situation, there is a critical Rayleigh number, below which the fluid is at rest, and heat transfer is by pure conduction only. Because we have not found in the literature a linear stability analysis of the influence of a magnetic field on the Benard flow within an infinite horizontal porous layer heated from below, we include a brief outline here. The problem is self adjoint, so the principle of exchange of stability holds. Thus, the time derivative in the governing equations does not need to be considered. The linearized local forms of Equations 5–7 for small perturbations about the conductive state are as follows:

$$a\frac{\partial^2 \hat{u}}{\partial x^2} + \frac{\partial^2 \hat{u}}{\partial y^2} = -R\frac{\partial^2 \hat{T}}{\partial y^2} \tag{25}$$

$$\nabla^2 \hat{T} = \hat{u} \tag{26}$$

where the superscript $\hat{}$ indicates perturbations from the pure conduction state, and $a = (1 + \mathrm{Ha}^2)$. The above equations must satisfy the following boundary conditions:

$$\hat{u} = \hat{T} = 0 \qquad \text{at} \qquad x = 0,\ 1 \tag{27}$$

The solution to Equations 25–27 is obtained by assuming the following:

$$\hat{u} = U(x)e^{i\alpha y} \qquad \hat{T} = T(x)e^{i\alpha y} \tag{28}$$

Substituting Equation 28 into Equations 25 and 26 and eliminating U from the resulting equations, we obtain the following:

$$a\theta^{\mathrm{IV}} - \alpha^2(a+1)\theta^{\mathrm{II}} + \alpha^4\theta = \mathrm{R}\alpha^2\theta \tag{29}$$

This equation admits solutions of the form $\theta = C\sin(n\pi y)$, where C is an arbitrary constant and n an integer so that the boundary condition, Equation 27, is satisfied.

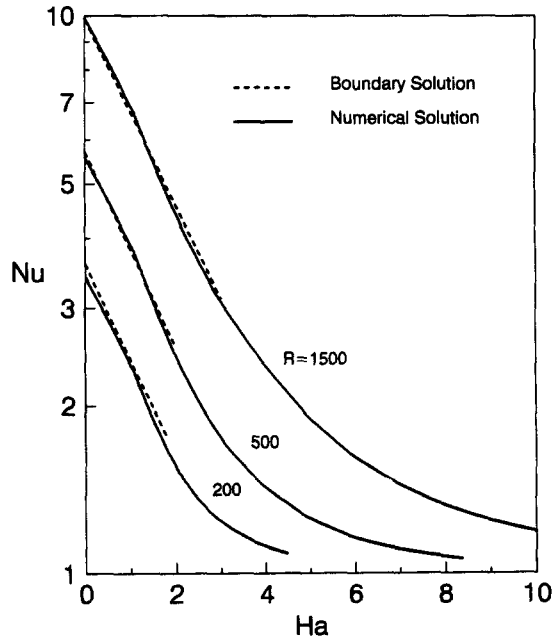

Figure 4 Effect of the Hartmann number on the Nusselt number for $\theta = 90°$ and various values of the Rayleigh number

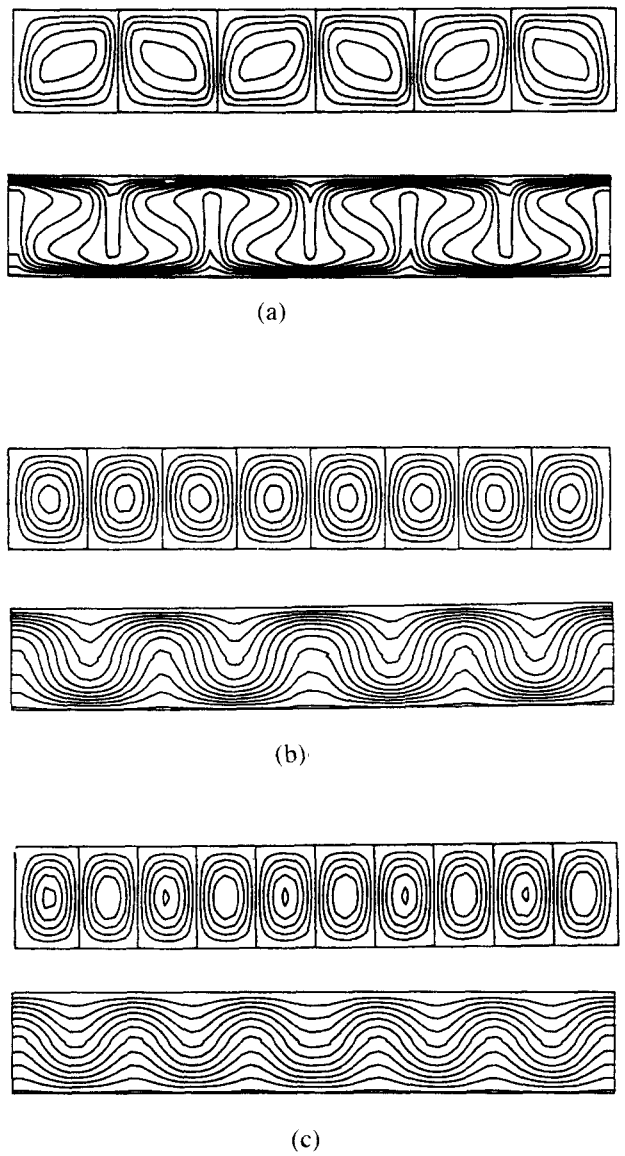

Figure 5 Computed contour maps of the streamfunction and isothermal lines for a horizontal cavity heated from below ($\theta = 180°$) for $A = 6$, $R = 500$, and a) $Ha = 0$, $\psi_{max} = 15.400$; b) $Ha = 4$, $\psi_{max} = 3.031$; c) $Ha = 5$, $\psi_{max} = 1.581$

Substituting θ into Equation 29, it is readily found that the assumed flow is neutrally stable when

$$R_{cr} = \frac{an^4\pi^4 + \alpha^2(a+1)n^2\pi^2 + \alpha^4}{\alpha^2} \qquad (30)$$

so that the minimum value occurs at $n = 1$ and $\partial R_{cr}/\partial\alpha = 0$, that is, when

$$R_{cr} = \left(1 + \sqrt{Ha^2 + 1}\right)^2 \pi^2, \left[n = 1, \alpha = \pi(Ha^2 + 1)^{1/4}\right] \qquad (31)$$

In the absence of a magnetic field; i.e., when $Ha = 0$, the above results reduce to

$$R_{cr} = 4\pi^2, (n = 1, \alpha = \pi) \qquad (32)$$

which are the classical results obtained in the past by Lapwood (1948).

From Equations 31 and 32, it is observed that, in the limit of $Ha \gg 1$, the critical Rayleigh and wave numbers, R_{cr} and α_{cr}, are of order Ha^2 and $Ha^{-1/2}$, respectively. In the case of a pure fluid layer, it was demonstrated by Chandrasekhar (1961) that Ra_{cr} is also of order Ha_f^2 but, due to higher derivative order of the Newtonian dissipation, α was found to be of order $Ha_f^{-1/3}$ (where $Ra_f = R/Da$, $Ha_f = Ha/\sqrt{Da}$ and $Da = K/L^2$, see Vasseur et al. 1995). The effect of the Darcy number on the onset of motion within a porous layer heated from below by a constant heat flux or a constant temperature has been recently investigated by Alchaar et al. (1995) using the Brinkman model.

Figures 5a–c show typical streamlines and isotherms obtained numerically for $A = 6$, $R = 500$, and various values of Ha. In the absence of a magnetic field; i.e., when $Ha = 0$, it is seen from Figure 5a that six cells of approximately equal size and intensity occupy the width of the porous layer. The shape of the cells is observed to be skewed by the strong convection, $\psi_{max} = 15.40$, resulting from the relatively high R considered here. The large distortion of the isotherms in Figure 5a is also an indicator of the intensity of the convection within the fluid layer. A step increase in the strength of a magnetic field from $Ha = 0$ to 4 results in the response as shown in Figure 5b. The six-cells mode obtained for $Ha = 0$ is now replaced by a eight-cells pattern. This trend is in agreement with the linear-stability theory, Equation 31, according to which the effect of the magnetic field is to decrease the wavelength of the incipient cells $[\alpha = \pi(Ha^2 + 1)^{1/4}]$. Also, the strength of convection is considerably decreased by the drag induced by the magnetic field, as indicated by a weak distortion of the isothermal lines and the value of the maximum stream function, which is now only $\psi_{max} = 3.03$. As the Hartmann number is further increased, up to $Ha = 5$, ten cells of approximately equal size and intensity are now seen to occupy the width of the cavity. For this situation, the isotherms of Figure 5c indicate that the convective regime is very weak. In fact, this situation is very close to the purely diffusive regime, which, in an infinite porous layer, would occur according to Equation 31 when $Ha \geq 6$ and $R = 500$.

Figure 6 presents relationship between the average Nusselt number and the Hartmann number for the case with $A = 6$ and $R = 500$. Naturally, the heat transfer is maximum in the absence of a magnetic field, because the convection is maximum for this situation. In general, Nu decreases steeply with the imposition of an external magnetic field, because this latter considerably reduces, the strength of convection as discussed earlier. At $Ha \simeq 3.6$,

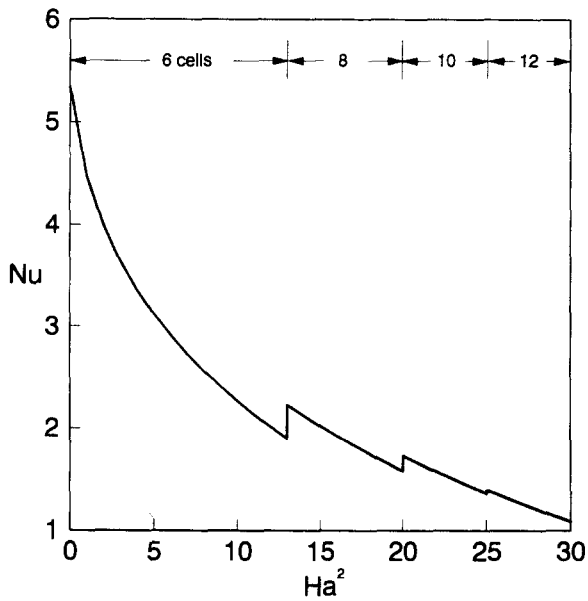

Figure 6 Nusselt number Nu *versus* Hartmann number Ha for $\theta = 180°$, $A = 6$ and $R = 500$

a slight increase of Nu is observed, which results from the transition in the number of cells within the cavity from six to eight. At Ha ≃ 4.5, another bifurcation from an eight-cell to a ten-cell pattern occurs. Afterwards, the convective motion is more and more inhibited by the magnetic drag. At Ha ≃ 5.0 a bifurcation from a ten-cell to a twelve-cell pattern occurs, but the convection is now so low (Nu ~ 1) that it does not affect the heat transfer.

The inclined cavity

The effect of a magnetic field on the natural convection heat transfer within a tilted cavity is now discussed. This problem, in the absence of a magnetic field, has been considered recently by Caltagirone and Bories (1985) and Moya et al. (1987). It was demonstrated by these authors that, at tilt angles close to zero, the preferred mode of circulation is multiple cell, while at greater tilt

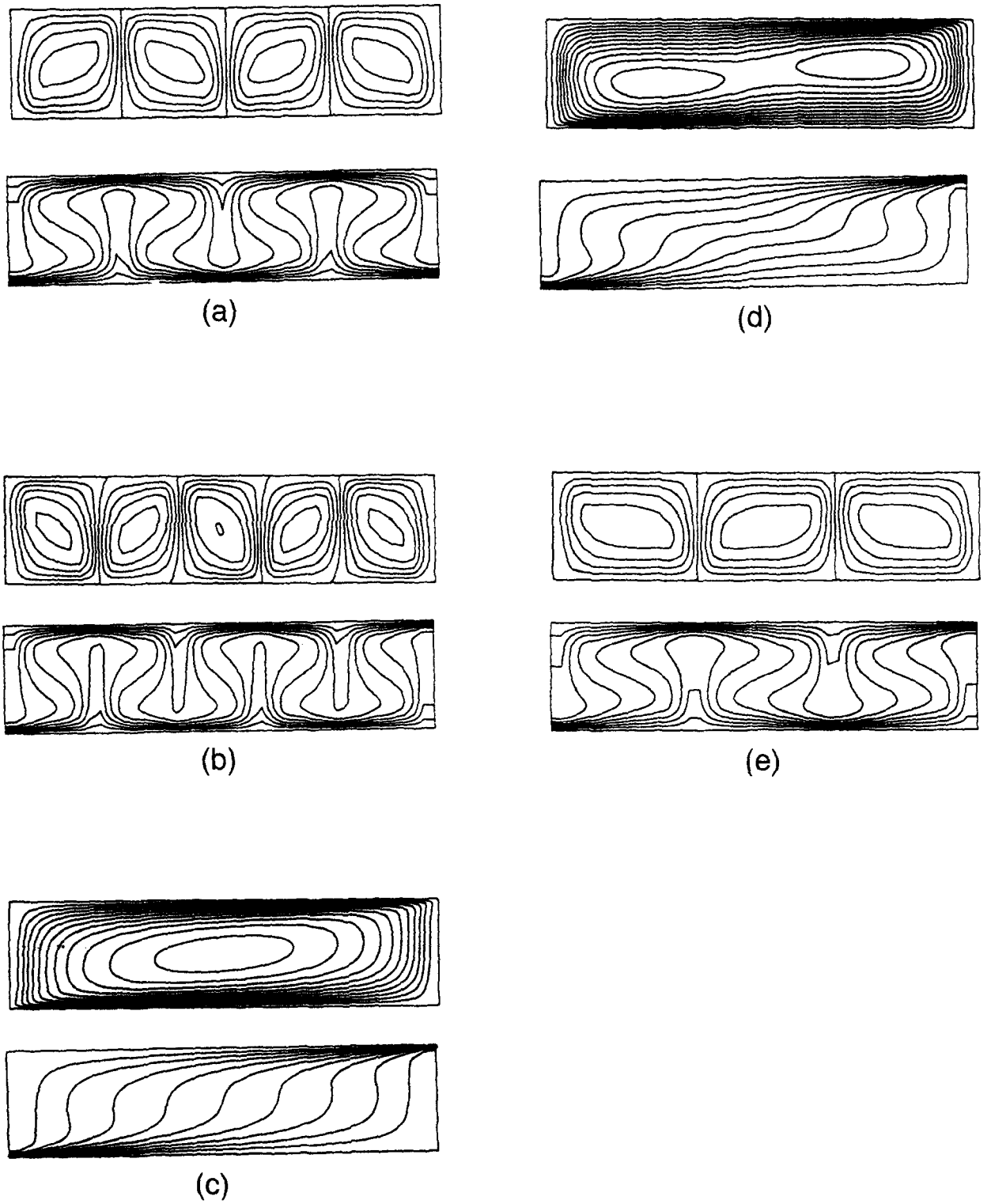

Figure 7 Computed contour maps of the streamfunction and isothermal lines for an inclined cavity for $A = 4$, Ha = 0 R = 500, and a) $\theta = 180°$, $\psi_{max} = 15.417$; b) $\theta = 175°$, $\psi_{max} = 15.671$; c) $\theta = 140°$, $\psi_{max} = 28.804$; d) $\theta = 171°$, $\psi_{max} = 17.733$; e) $\theta = 180°$, $\psi_{max} = 16.156$

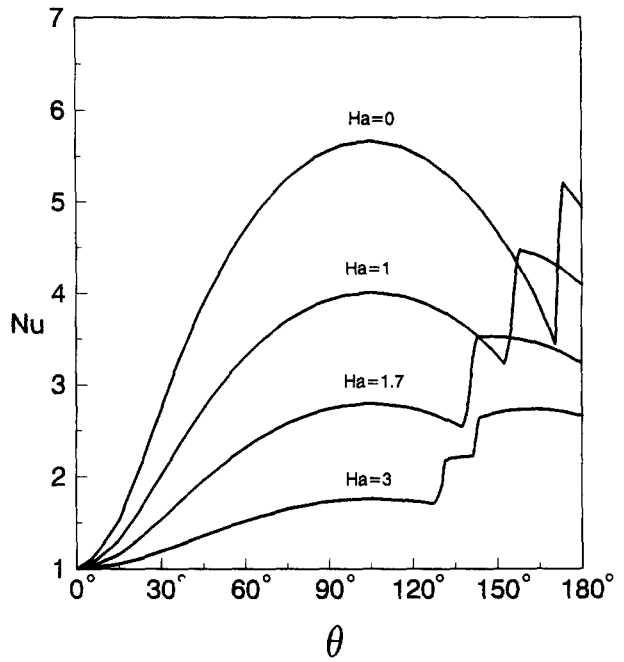

Figure 8 Effect of inclination angle on the Nusselt number for $A = 4$, $R = 500$, and various values of the Hartmann number

angles, the preferred mode is single cell. The transition angle from multiple- to single-cell convection patterns was shown to depend on the aspect ratio and the Rayleigh number. This phenomenon is illustrated in Figure 7, where the streamlines are shown for $A = 4$, R = 500, and various values of the inclination angle θ. When the cavity is horizontal ($\theta = 180°$), Figure 7a shows that four cells develop with alternate directions of rotation (Benard's cells). As the inclination angle θ is decreased to 175°, a five-cell convection is obtained, as illustrated by Figure 7b. At this stage, a remark must be made with regard to the numerical procedure followed here. To speed up the computational procedure, the converged velocity and temperature fields, obtained from a numerical run with a given inclination angle θ, were used as initial conditions for another run with a small change in the tilt angle. In this way, it was found that the five-cell convection prevails up to $\theta > 140°$. For smaller tilt angles, an evolution from multiple cells to single-cell convection is observed. Thus, for $\theta = 140°$, the flow in Figure 7c is characterized by a single cell, where all the fluid inside the porous material circulates in the same sense and the streamfunction has only one extreme value.

In the transitional region between multiple- and single-cell convection, flow hysteresis effects were observed in the present study. Thus, when the inclination angle increased from $\theta = 140°$ back to $\theta = 180°$, the flow field did not revert to the previous solutions for the same θ. For example, the single-cell solution observed for $\theta = 140°$ could be maintained up to $\theta = 170°$. Increasing θ to 171°, it is found that the flow now consists of one main cell with secondary cells developing within. This type of flow pattern, illustrated in Figure 7d, has been observed in the past by Moya et al. (1987). As the tilt angle is increased further, three cells develop with alternate directions of rotation and are maintained up to $\theta = 180°$ (Figure 7e). To the author's knowledge, this flow "hysteresis" has not been observed in the past.

The average Nusselt number Nu for aspect ratio of four and for several Hartmann numbers is shown in Figure 8 as a function of the tilt angle. As the inclination θ approaches 0°, the Nusselt number tends toward unity, indicating that the heat transfer is mainly due to conduction. This is expected, because $\theta = 0°$ corresponds to the case of a cavity heated from the top, which causes no convection, because the density gradient is stable. Most of the change in the heat transfer occurs in the range $0° < \theta < 90°$, where the cavity is heated from the top. Also, it is observed that, for a given inclination angle, the Nusselt number decreases with an increase of the Hartmann number, because the convection is considerably decreased with the application of the magnetic field. As the inclination angle is increased above 90°, the enclosure starts to be heated from the bottom. Each curve passes through a maximum that depends upon Ha. As demonstrated by Moya et al. (1987), the peak in Nusselt number occurs approximately at an inclination angle for which the most vigorous convection flow is developed. As the inclination angle is increased further, the curves are seen to pass through a second maximum. Contrary to the case of the first maximum, which was obtained for a single-cell mode, the second maximum is due to the appearance of a multiple-cell convection. The transition angle from single- to multiple-cell convection patterns depends strongly upon the magnetic field. For instance, a transition from one-cell to three-cell pattern occurs at $\theta = 171°$ when $Ha = 0$ but it is at about $\theta = 141°$ when $Ha = 1.7$. Therefore, the second peak in Nusselt number takes place at a lower transition angle when the Hartmann number is increased. Also, Figure 8 indicates that, for $Ha = 3$, not only there is a transition from one-cell to three-cell pattern at $\theta \simeq 131°$ but a second transition from three-cell to five-cell pattern occurs at $\theta \simeq 143°$. Naturally, due to the flow hysteresis discussed before, the transition angles obtained when the inclination angle is decreased from $\theta = 180°$ toward 0° are different from those of Figure 8. From the numerical results (not presented here) it was found that the transition from multiple- to single-cell convection generally occurred at lower angles. For example, when $Ha = 0$, a transition angle $\theta \simeq 140°$ was obtained. Finally, it must be mentioned that the occurrence of the first maximum, for the single-cell mode, was not affected by the hysteresis effect.

Conclusions

The effect of a transverse magnetic field on buoyancy-driven convection in an inclined rectangular porous cavity, saturated with an electrically conducting fluid, was studied both numerically and analytically. The main conclusions of this study are summarized as follows:

1. In the case of a vertical cavity heated from the side ($\theta = 90°$), it is shown that a simple dimensional analysis can correctly predict the asymptotic behavior of the velocity field in the limit $R \to \infty$. Also, in the boundary-layer regime, the dependence of the Nusselt number on R, A, and Ha is obtained explicitly following the integral approach of Simpkins and Blythe (1980). The resulting expression, $Nu = 0.51[R/A(1 + Ha^2)]^{1/2}$ was confirmed by comparing the numerical results obtained for cavities with aspect ratios $A = 4$ and 8.

2. The effect of a magnetic field on the Benard convection, within a porous layer heated from below $\theta = 180°$ has been considered. The critical Rayleigh number for the onset of convection has been predicted, using a linear stability theory. For supercritical convection, the adjustment of the roll pattern, after a change in the Hartmann number, is illustrated for a given Rayleigh number and a cavity with an aspect ratio $A = 6$. Results for the heat transfer as a function of Ha are presented.

3. The effect of the orientation angle on the present problem was found to be considerable. The transition angle from single cell- to multiple-convection pattern is considerably affected by the imposition of a magnetic field. Thus, for a cavity with R = 500 and

$A = 4$, the transition angle is $\theta = 171°$ when $Ha = 0$, but it is $\theta = 131°$ when $Ha = 3.0$.

Acknowledgments

This work was supported in part by the Natural Sciences and Engineering Research Council of Canada and jointly by the FCAR Government of Quebec.

References

Alchaar, S., Vasseur, P. and Bilgen, E. 1995. Effects of a magnetic field on the onset of convection in a porous medium, *Warme- und Stoffübertragung*, **30**, 259–267

Bejan, A. 1985. The method of scale analysis: Natural convection in a porous medium. In *Natural Convection: Fundamentals and Applications*, S. Kakac et al. (eds.), Hemisphere, Bristol, PA

Caltagirone, J. P. and Bories, S. 1985. Solutions and stability criteria of natural convection flow in an inclined porous layer, *J. Fluid Mech.*, **155**, 267–287

Chandrasekhar, S. 1961. *Hydrodynamic and Hydromagnetic Stability*, Clarendon, Oxford, UK

Garandet, J. P., Alboussiere, T. and Moreau, R. 1992. Buoyancy-driven convection in a rectangular enclosure with a transverse magnetic field. *Int. J. Heat Mass Transfer*, **35**, 741–748

Gill, A. E. 1966. The boundary-layer regime for convection in a rectangular cavity. *J. Fluid Mech.*, **26**, 515–536

Klarsfeld, S. 1970. Champs de temperature associes aux mouvements de convection naturelle dans un milieu poreux limite. *Rev. Gen. Thermique*, **108**, 1403–1423

Kumar Jha, B. and Prasad, R. 1991. MHD free-convection and mass transfer flow through a porous medium with heat source. *Astrophys. Space Sci.*, **8**, 117–123

Lapwood, E. R. 1948. Convection of a fluid in a porous medium. *Proc. Cambridge Philos. Soc.*, **44**, 508–521

Lauriat, G. and Prasad, 1987. Natural convection in a vertical porous cavity: A numerical study for Brinkman-extended Darcy formulation. *J. Heat Transfer*, **109**, 688–696

Moya, S. L., Ramos, E. and Sen, M. 1987. Numerical study of natural convection in a tilted rectangular porous material. *Int. J. Heat Mass Transfer*, **30**, 741–756

Ni, J., Beckermann, C. and Smith, T. F. 1993. Effect of an electromagnetic field on natural convection in porous media, *Fundamentals of Heat Transfer in Electromagnetic, Electrostatic and Acoustic Fields*, ASME HTD, **248**, 23–33

Nield, D. A. and Bejan, A. 1992. Convection in porous media, Springer-Verlag, Berlin

Patankar, S. V. 1980. *Numerical Heat Transfer and Fluid Flow*, B. J. Smith et al. (eds.). Hemisphere, Bristol, PA

Prasad, V. and Kulacki, F. A. 1984. Convective heat transfer in a rectangular porous cavity-effect of aspect ratio on flow structure and heat transfer. *J. Heat Transfer*, **106**, 158–165

Raptis, A., Massalas, C. and Tzivanidis, G. 1982a. Hydromagnetic free convection flow through a porous medium between two parallel plates. *Phys. Lett.*, **90A**, 288–289

Raptis, A. and Vlahos, J. 1982b. Unsteady hydromagnetic free convective flow through a porous medium. *Lett. Heat Mass Transfer*, **9**, 56–64

Seki, N., Fukusako, S. and Inaba, H. 1978. Heat transfer in a confined rectangular cavity packed with porous media. *Int. J. Heat Mass Transfer*, **106**, 152–157

Shiralkar, G. S., Haajizadeh, M. and Tien, C. L. 1983, Numerical study of high Rayleigh number convection in a vertical porous enclosure, *Num. Heat Transfer*, **6**, 223–234

Simpkins, P. G. and Blythe, P. A. 1980, Convection in a porous layer, *Int. J. Heat Mass Transfer*, **23**, 881–887

Singh, A. K. and Dikshit, C. K. 1987, Natural convection effects of hydromagnetic generalised couette flow in a porous medium, *Ind. J. Theoret. Phys.*, **35**, 331–335

Takhar, H. S. and Ram, P. C. 1992, Effects of hall current of hydromagnetic free-convective flow through a porous medium, *Astrophys. Space Sci.*, **192**, 45–51

Vasseur, P., Hasnaoni, M., Bilgen, E. and Robillard, L. 1995, Natural convection in an inclined fluid layer with a transverse maganetic Field: Analogy with a porous medium, *J. Heat Transfer*, **117**, 1–9

Walker, K. L. and Homsy, G. M. 1978, Convection in a porous cavity, *J. Fluid Mech.*, **87**, 449–474

Weber, J. W. 1975, The boundary-layer regime for convection in a vertical porous layer, *Int. J. Heat Mass Transfer*, **18**, 569–573